

Original article

Numerical simulation and thermo-hydro-mechanical coupling model of in situ mining of low-mature organic-rich shale by convection heating

Jing Zhao^{1,2}, Lei Wang^{1,2}*, Shimin Liu³, Zhiqin Kang^{1,2}, Dong Yang^{1,2}, Yangsheng Zhao^{1,2}

¹Key Laboratory of In-situ Property Improving Mining of Ministry of Education, Taiyuan University of Technology, Taiyuan 030024, P. R. China

²The In-situ Steam Injection Branch of State Center for Research and Development of Oil Shale Exploitation, Taiyuan University of Technology, Taiyuan 030024, P. R. China

³Department of Energy and Mineral Engineering, G3 Center and Energy Institute, The Pennsylvania State University, University Park, PA 16802, USA

Keywords:

Convection heating
thermo-hydro-mechanical coupling
mathematical model
numerical simulation

Cited as:

Zhao, J., Wang, L., Liu, S., Kang, Z., Yang, D., Zhao, Y. Numerical simulation and thermo-hydro-mechanical coupling model of in situ mining of low-mature organic-rich shale by convection heating. *Advances in Geo-Energy Research*, 2022, 6(6): 502-514.
<https://doi.org/10.46690/ager.2022.06.07>

Abstract:

The in situ efficient exploitation of low-mature organic-rich shale resources is critical for alleviating the current oil shortage. Convection heating is the most critical and feasible method for in situ retortion of shale. In this study, a thermo-hydro-mechanical coupling mathematical model for in situ exploitation of shale by convection heating is developed. The dynamic distribution of the temperature, seepage, and stress fields during the in situ heat injection of shale and the coupling effect between multiple physical fields are studied. When the operation time increases from 1 to 2.5 years, the temperature of most shale formations between heat injection and production wells increases significantly (from less than 400 to 500 °C), which is a period of significant production of shale oil and pyrolysis gas. The fluid pore pressure gradually decreases from the peak point of the heat injection well to the surrounding. Compared with shale formation, bedrock permeability is poor, pore pressure increases slowly, and a lag phenomenon exists. The pore pressure difference between bedrock and shale is minimal by 1 year. When the heat injection time is 2.5 years, the permeability coefficient of shale formation in the area from the heat injection well to the production wells increases nearly 100 times the initial permeability coefficient. With increasing formation temperature, the vertical stress gradually evolves from compressive stress to tensile stress. Meanwhile, the action area of tensile stress expands outward with time with the heat injection well as the center. In general, increasing tensile stress enlarges the pore volume. It extends the fracture width, creating favorable conditions for the injection of high-temperature fluids and the production of oil and gas.

1. Introduction

Low-mature organic-rich shale is a fine-grained sedimentary rock rich in solid organic matter (kerogen). The internal organic matter is insoluble in conventional organic solvents. Therefore, shale gas and shale oil can only be generated through dry distillation (anaerobic pyrolysis). After shale oil hydrocracking, gasoline, kerosene, and diesel oil can be obtained (Bansal et al., 2019; Sun et al., 2019; Suganuma et

al., 2020). China's low-mature organic-rich shale reserves are enormous, equivalent to 57 billion tons of shale oil reserves. The in situ high-efficiency exploitation of shale is critical for alleviating the current oil shortage (Kang et al., 2020; Wang et al., 2020; Sultana et al., 2022). According to different heat sources, in situ heating methods of shale can be divided into conduction, convection, and radiation heating (Lin et al., 2016; Saif et al., 2019). Low-mature organic-rich shale is a dense, low-permeability rock with poor thermal conductivity in its

natural state. Only when external heat is transferred to the rock mass quickly can the development cost of shale be reduced and the efficient pyrolysis of shale be realized. However, the process of retorting shale by conduction heating is very slow, and the active migration ability of oil and gas is poor. Hence, a large amount of oil and gas is retained in the orebody and is challenging to be recovered. The convection heating technology mainly injects high-temperature and high-pressure fluid into the orebody. The fluid gradually heats an extensive range of orebody through fractures formed by fracturing and thermal cracking. Meanwhile, high-temperature fluid can carry oil and gas products for drainage and production, enabling its active migration ability. Based on this, experts generally believe that convection heating is the most important and feasible technology for in situ retortion of low-mature organic-rich shale.

During in situ exploitation of shale by convection heating, there are complex relationships among the seepage, stress, and temperature fields. The process is a typical thermo-hydro-mechanical coupling problem (Wang et al., 2021; Wilkins et al., 2021). The main coupling factors are as follows: 1) when fluid percolates in a shale formation, heat carried by a high-temperature fluid is transferred to a rock mass through conduction and convection, directly affecting the temperature field distribution in the rock mass. On the other hand, the fluid deforms the rock mass due to pore pressure and changes the formation stress field. 2) The temperature field change in shale formation significantly changes the porosity and permeability of the formation as well as fluid density, dynamic viscosity, and other parameters, directly influencing the seepage field distribution. On the other hand, the temperature change causes additional thermal stress in the rock mass. Moreover, the density, elastic modulus, and specific heat of shale are all functions of temperature; therefore, the temperature change redistributes the stress field. 3) The stress field change in shale formation significantly alters the opening of fractures and pores, affects the porosity and permeability of the formation, and changes the seepage field.

Previous studies on numerical simulation mainly focus on in situ shale mining technology by conduction heating. Rao et al. (2021) studied a general physics-based data-driven framework for numerical simulation. Pei et al. (2018) simulated the conversion process of in situ electric heating assisted by nitrogen injection. Compared with traditional in-situ conversion process technology, adding nitrogen can increase the heating rate of shale formation and production, which can be attributed to the improved thermal convection, pressurization effect, and gas-driving mechanism. Kelkar et al. (2014) established a thermohydronechanical coupling mathematical model to simulate the in situ shale pyrolysis process but only considered oil and gas multiphase fluid after kerogen pyrolysis rather than the externally injected fluid.

After a comprehensive study of various patented technologies and the characteristics of shale, Taiyuan University of Technology (Zhao et al., 2005; Liang et al., 2021; Yang et al., 2021) proposed the technology of shale pyrolysis by high-temperature water vapor (MTI Technology). The technology uses high-temperature water vapor as the heat carrier to heat

shale and carries oil and gas to the surface through water vapor.

Although the thermal recovery technology for heavy oil by steam injection has achieved good economic benefits, shale deposits are different in sedimentary environment, geological structure, physical properties, chemical properties, mineral composition, and seepage characteristics compared with traditional heavy oil reservoirs (Shabdirova et al., 2019; Sun et al., 2021). Therefore, applying the previous heavy oil thermal recovery theory is infeasible. In this study, a thermo-hydro-mechanical coupling mathematical model for in situ exploitation of shale is developed by combining rock mechanics, heat transfer, and seepage mechanics, considering relevant factors as much as possible. Based on the developed model, numerical simulations are performed. The coupling model has the following advantages: permeability is a function of volume stress, pore pressure, and temperature. The energy conservation equation takes into account the effects of fluid conduction, convection, and water vapor phase change heat transfer, and the model is more practical. In order to more accurately simulate the in-situ pyrolysis process, the heat transfer, seepage and mechanical parameters used in the simulation are obtained through laboratory tests. As a result, the dynamic distribution law of temperature, seepage, and stress fields is obtained during in situ shale mining by heat injection. In addition, the coupling effect between multiple physical fields is discussed, providing a reference for the technological development of in situ shale mining by heat injection for field practice.

2. Mathematical model for in situ exploitation of low-mature organic-rich shale

2.1 Basic assumptions

In situ shale mining for oil and gas recovery by heat injection is a highly complex physical and chemical process involving a multiphase mixed seepage of steam, liquid water, oil and gas, heat transfer, solid deformation, thermal fracture, fluid-phase change, the change of physical parameters of each phase fluid and shale with temperature, and high-temperature pyrolysis of shale. Therefore, to ensure that the mathematical model not only reflects the physical essence of the problem but is also comprehensively simple and feasible to solve, this study introduces the following basic assumptions:

1) Compared with traditional reservoirs, shale oil content is extremely low (average is 5%); hence, the flow of a minimal amount of shale oil and cracking gas can be ignored in in situ shale mining by heat injection. The steam is injected into the shale formation from the beginning till the end, and the content has an absolute advantage. Therefore, it can be considered that the seepage channel is completely saturated by water vapor and liquid water.

2) Due to the control of multiple physical and chemical factors, the two miscible fluids (liquid water vapor and water) in the seepage channel are interpenetrating, containing, and disorderly distributed (Avraam and Payatakes, 1995; Akinlua and Smith, 2009; Montgomery et al., 2013; Yang et al., 2019). Hence, the relative permeability and the specific phase interface position at a particular time cannot be determined, and the

vapor–liquid phase cannot be completely separated. However, according to the temperature distribution from high to low, we believe that water vapor is dominant in the high-temperature section and water is prevalent in the low-temperature section.

Based on the above principle, it is assumed that the relative saturation of water vapor is S_g and that of liquid water is S_w , both of which meet the following requirements:

$$S_g + S_w = 1 \quad (1)$$

Among them:

$$\begin{cases} S_g = \frac{T - T_0}{T_1 - T_0} \\ S_w = 1 - S_g = \frac{T_1 - T}{T_1 - T_0} \end{cases} \quad (2)$$

where T_1 represents the initial temperature of high-temperature steam, T_0 represents the original temperature of the formation, and T represents the temperature at a particular position between T_1 and T_0 .

3) Neglecting the effect of surface tension at the vapor and liquid interface, the gas pressure on both sides of the interface is the same as the liquid pressure.

4) The vapor and liquid percolation in shale follow the linear Darcy's law in micro pressure gradient. According to the main seepage direction, the constitutive seepage equation is as follows:

$$\Delta q_i = \frac{k_{ij}}{\mu_h} \Delta \frac{\partial q}{\partial x_j} \quad (3)$$

In the entire seepage interval, the equation is as follows:

$$q_i = \frac{k_{ij}}{\mu_h} \frac{\partial q}{\partial x_j} \quad (4)$$

where $q_i (i = x, y, z)$ is the two-phase flow rate per unit time in x, y, z directions, respectively, $k_{ij} = k_{ij}(\Theta, p, T)$, permeability k_{ij} is a function of volume stress, pore pressure p , and temperature T ; μ_h is the dynamic viscosity of the vapor-liquid two-phase mixed fluid.

5) Water vapor is treated as a nonisothermal process, and the state equation of water vapor is:

$$\rho_g = \frac{Mp}{RTZ} \quad (5)$$

where ρ_g represent the densities of water vapor, M represents the molecular weight of water vapor, R represents the gas constant, and Z represents the compression factor.

6) The density, dynamic viscosity, heat conductivity, and specific heat of water vapor and liquid water with temperature are considered.

7) The porosity, density, thermal conductivity, and specific shale heat are considered temperature functions.

8) The local thermal equilibrium between the fluid and solid is instantaneously achieved, and the temperature of the two is considered equal at the same position (Saurel and Abgrall, 1999).

9) The temperature (optimum pyrolysis temperature is 300–500 °C) is used to determine whether the shale has been cracked to select its complete pyrolysis range.

10) Low-mature organic-rich shale can be simplified as

continuous medium rock mass, which fully satisfies the stress equilibrium and constitutive elasticity equations and follows the modified Terzaghi effective stress law (Nur and Byerlee, 1971; Gelet et al., 2012). Thus, the influence of thermal stress should be considered:

$$\sigma = \bar{\sigma} - \alpha p \mathbf{1} - \omega T \mathbf{1} \quad (6)$$

where $\bar{\sigma}$ represents the effective stress tensor, σ represents the total stress tensor, α represents the Biot effective stress coefficient, $\mathbf{1}$ represents the second-order identity tensor, ω represents the thermoelastic effective stress coefficient, $\omega = (\lambda + 2/3G)\beta$, where G and λ are called lame constants and β represents the volumetric thermal expansion coefficient.

2.2 Seepage equation of vapor–liquid two-phase mixed fluid

According to hypothesis 2), the vapor-liquid two-phase flow is exceptionally complex under high temperature, high pressure, and chemical reaction. Therefore, there is a large error when using the existing two-fluid model to describe the flow separately, and many coupling parameters are involved, making it difficult to solve. Based on this, a seepage mathematical model of vapor-liquid two-phase is developed. A unified equation is used to reflect the seepage law of vapor-liquid two-phase in the in situ shale mining process by heat injection.

The two-phase fluid in porous media is treated as a binary mixture, and steam and liquid water are defined as two inseparable components. Therefore, their mixture can be regarded as a single fluid medium with a stable change in physical composition (Li et al., 2005; Raeini et al., 2012). The two-phase mixing model is advantageous because it is closer to reality, and the two fluids determine the flow rate and pressure of the fluid. In addition, the number of equations to be solved in the two-phase mixture model is reduced by at least half, and the two-phase mixture component is retained, simplifying the solution computation. The equivalent physical parameters of the two-phase mixture, such as density, dynamic viscosity, conductivity, and specific heat, are closely related to their relative saturation, which can be obtained by the weighted average of the corresponding parameters of the two components. The following is a detailed mathematical model derivation of vapor-liquid two-phase mixed seepage.

According to the mass conservation principle (Salimzadeh et al., 2018), the continuity equation of two-phase flow is obtained as follows:

$$\text{div}(\rho q_i) = \frac{\partial(\rho n)}{\partial t} \quad (7)$$

The component form is as follows:

$$\frac{\partial(\rho_h q_x)}{\partial x} + \frac{\partial(\rho_h q_y)}{\partial y} + \frac{\partial(\rho_h q_z)}{\partial z} = \frac{\partial(\rho_h n)}{\partial t} \quad (8)$$

where ρ_h represents the density of vapor-liquid mixture, n represents the porosity of shale, and t represents time.

The following two equations express the density and dynamic viscosity of the two-phase mixed fluid:

$$\rho_h = S_g \rho_g + S_w \rho_w \quad (9)$$

$$\mu_h = S_g \mu_g + S_w \mu_w \quad (10)$$

where ρ_w represent the densities of liquid water, respectively, and μ_g and μ_w represent the dynamic viscosity of water vapor and liquid water, respectively.

Considering the compressibility of water vapor, there are:

$$\frac{\partial \rho_w}{\partial t} = \beta \rho_w \frac{\partial p}{\partial t} \quad (11)$$

By substituting Eqs. (4), (9), (10) and (11) into Eq. (8), we can obtain:

$$\begin{aligned} & \left(\frac{S_g M p + S_w \rho_w R T Z}{S_g \mu_g R T Z + S_w \mu_w R T Z} \right) \left(K_x \frac{\partial^2 p}{\partial x^2} + K_y \frac{\partial^2 p}{\partial y^2} \right) \\ & = \left(\frac{n S_g M}{R T Z} + n S_w \beta \rho_w \right) \frac{\partial p}{\partial t} \end{aligned} \quad (12)$$

Eq. (12) is the final form of the seepage mathematical model of vapor-liquid two-phase mixing.

2.3 Energy conservation equation

Many pores and fractures are produced in the pyrolytic shale formation; hence, the solid skeleton and fluid exist in the same volume. However, they have different thermal dynamic characteristics, such as specific heat and thermal conductivity. Therefore, solid skeleton and fluid energy conservation equations must be defined separately (Wei et al., 2019; Wopara, 2021).

The energy conservation equation of a solid shale skeleton is defined as follows:

$$(1-n)(\rho_s c_s) \frac{\partial T}{\partial t} = (1-n) \lambda_s \nabla^2 T + q_s \quad (13)$$

where ρ_s represents shale density, c_s represents the specific heat of shale, λ_s represents the thermal conductivity of shale, and q_s represents a solid heat sink.

For vapor-liquid two-phase flow, the corresponding energy conservation equation can be defined as follows:

$$n \rho_h c_h \frac{\partial T}{\partial t} + \rho_h c_h v_h \cdot \nabla T + n \rho_w l_w \frac{\partial S_w}{\partial t} = n \lambda_h \cdot \nabla^2 T + q_h \quad (14)$$

where c_h represents the specific heat of vapor-liquid two-phase mixed fluid, λ_h represents the heat conductivity of vapor-liquid two-phase mixed fluid, v_h represents the velocity of vapor-liquid two-phase mixed fluid, l_w represents the latent heat of vaporization of water, and q_h represents the confluence of fluid heat source.

Similarly, the specific heat and heat conductivity of two-phase mixed fluid can be expressed using:

$$c_h = S_g c_g + S_w c_w \quad (15)$$

$$\lambda_h = S_g \lambda_g + S_w \lambda_w \quad (16)$$

The seepage flow is subject to Darcy's law.

Therefore, after substituting Eqs. (9), (10), (15), and (16) into Eq. (14), we obtain:

$$\begin{aligned} & \frac{(S_g \rho_g + S_w \rho_w)(S_g c_g + S_w c_w)}{S_g \mu_g + S_w \mu_w} (k_i \nabla p) \cdot (\nabla T) + \\ & n \rho_w l_w \frac{\partial S_w}{\partial t} + n (S_g \rho_g + S_w \rho_w)(S_g c_g + S_w c_w) \frac{\partial T}{\partial t} \\ & = n (S_g \lambda_g + S_w \lambda_w) \cdot \nabla^2 T + q_h \end{aligned} \quad (17)$$

Based on assumption 8), the solid skeleton and the two-phase mixed fluid are always in a state of thermal equilibrium. Therefore, Eqs. (15) and (19) can be combined to obtain a unified energy conservation equation as shown below:

$$\begin{aligned} & (\rho c)_t \frac{\partial T}{\partial t} + \frac{(S_g \rho_g + S_w \rho_w)(S_g c_g + S_w c_w)}{S_g \mu_g + S_w \mu_w} (k_i \nabla p) \cdot (\nabla T) \\ & + n \rho_w l_w \frac{\partial S_w}{\partial t} = \lambda_t \nabla^2 T + q_t \end{aligned} \quad (18)$$

where $(\rho c)_t$, λ_t , and q_t are equivalent heat capacity, heat conductivity, and source-sink phase of shale filled with two-phase fluid, respectively. In addition:

$$(\rho c)_t = n(S_g \rho_g + S_w \rho_w)(S_g c_g + S_w c_w) + (1-n)(\rho_s c_s) \quad (19)$$

$$\lambda_t = n(s_g \lambda_g + s_w \lambda_w) + (1-n)\lambda_s \quad (20)$$

$$q_t = q_h + q_s \quad (21)$$

In Eq. (20), the first term is the energy change caused by temperature change, the second is the energy change caused by fluid convection, the third is the energy change caused by the phase transition of water vapor, the fourth is the energy change caused by heat conduction, and the fifth is the source item.

Therefore, Eqs. (20)-(23) constitute the energy conservation equation of in situ shale mining by heat injection.

2.4 Deformation equation of rock mass

According to basic elasticity theory, the static equilibrium equation of the matrix rock mass is as follows (Tong et al., 2010; War and Arneppalli., 2021; Wang et al., 2022):

$$\sigma_{i,j,j} + F_i = 0 \quad (22)$$

According to hypothesis 10), considering the effect of pore pressure and thermal expansion stress, the stress balance equation is expressed by displacement:

$$(\lambda + G)u_{j,ji} + Gu_{i,jj} - \alpha P_i - \omega T_i + F_i = 0 \quad (23)$$

2.5 Hydro-thermo-mechanical coupling model

Based on the coupling analysis of fluid flow, heat transfer, rock deformation, and other factors, the thermo-hydro-mechanical coupling equation of low mature organic-rich shale in situ mining by heat injection is established.

Supplementing the above mathematical model with necessary initial and boundary conditions, a complete thermo-hydro-mechanical coupling mathematical model of in situ shale mining by heat injection is developed. The above model is a set of highly complex nonlinear equations, and their coefficients also contain nonlinear terms. For such a complex differential equation, its analytical solution cannot be obtained directly

but can only be solved using a numerical method to find its approximate solution:

Compared with the uncoupled model, the coupling model has the following characteristics:

1) Permeability k_{ij} is a function of volume stress, pore pressure, and temperature. $k_{ij} = k_{ij}(\Theta, p, T)$.

2) The energy conservation equation considers the effects of fluid conduction, convection, and heat transfer of water vapor phase change. As a result, the model is more practical.

3) The effect of pore pressure and thermal stress is considered in the solid deformation equation.

4) The physical parameters of fluid (saturation, density, dynamic viscosity, specific heat, thermal conductivity, etc.) and shale (density, specific heat, thermal conductivity, porosity, etc.) in the above coupled governing equations are all temperature functions.

Galerkin finite element method is used to solve the coupling model. The main idea is to perform a time cycle for different fields. In each cycle, each field is analyzed separately and then relevant parameters are solved by coupling iteration. The specific design process is as follows. (i) According to the existing initial and boundary conditions, calculate the temperature field distribution in shale at t_0 to obtain the relative saturation of vapor-liquid two-phase fluid. Simultaneously, the physical property parameters of fluid and shale are reassigned according to the temperature, and the resulting parameters are substituted into the seepage equation. (ii) The fluid pressure and velocity are calculated by the seepage equation and substituted into the rock mass deformation equation. (iii) Calculate the stress field distribution of the rock mass under dead weight stress, pore pressure, and thermal stress to obtain the permeability coefficient of shale formation under volume stress, pore pressure, and temperature. (iiii) $t = t_0 + \Delta t$ Repeat the previous steps for calculation.

3. Model validation

The accuracy of the multi field coupling mathematical model and Fortran calculation program in this paper is verified by an example. Biot et al. (1941) analyzed the fluid solid coupling problem of a sand column and gave an analytical solution of isothermal elastic consolidation. Based on the THM coupling program used in this paper, the isothermal fluid solid coupling consolidation problem is calculated. The calculated results are in good agreement with the analytical solution (Fig. 1), which shows the reliability of the mathematical model and calculation program in this paper. The rock parameters used in the calculation example are: elastic modulus is 6×10^3 Pa, Poisson's ratio is 0.4, Biot coefficient is 1, porosity is 20%, permeability is 4×10^{-4} m².

4. Numerical simulation of in situ mining of low-mature organic-rich shale

The developed mathematical model is compiled using the FORTRAN programming language. A numerical simulation of a well group (one heat injection well and eight production wells) with a "nine-point method" well layout of in situ shale mining by water vapor injection is performed to obtain the va-

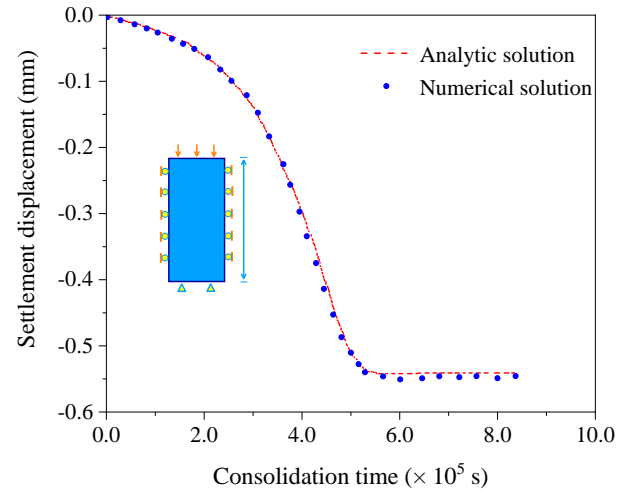


Fig. 1. Comparison between calculation solution and analytical solution.

riation law of temperature, seepage, and stress fields in the coupling development process for the well group under three-dimensional state.

4.1 Variation of physical parameters of steam, liquid water, and shale

The coupling of "physical parameters" is an integral part of the three-field coupling mechanism. Therefore, when implementing the three-field coupling theory, it is necessary to investigate the effect of temperature and pressure on many physical parameters of fluid and rock, especially density, viscosity, thermal conductivity, specific heat, and other parameters.

1) Effect of temperature and pressure on water vapor and liquid water density:

$$\rho_g = 2272.7 \times \frac{p \times 10^{-6}}{T + 273} \quad (24)$$

$$\rho_w = (0.9967 - 4.615 \times 10^{-5}T - 3.063T^2) \times 10^3 \quad (25)$$

where ρ_g and ρ_w represent the density of water vapor and liquid water, respectively, kg/m³; p represents pressure, Pa; T represents temperature, °C.

2) Effect of temperature on dynamic viscosity of water vapor and liquid water.

When the fluid makes a relative motion, it produces shear force in the interior to resist the relative fluid motion, called viscosity (Wang et al., 2019). The experimental results show that the dynamic viscosity of water vapor and liquid water varies with temperature and pressure but slightly changes with pressure and is extremely sensitive to temperature.

3) Effect of temperature on the specific heat of water vapor and liquid water:

$$c_g = -0.0001T^3 + 0.0948T^2 - 27.103T + 9246.8 \quad (26)$$

$$c_w = 0.0165T^2 - 1.4878T + 4207.4 \quad (27)$$

where c_w and c_g represent the specific heat of water vapor and liquid water, respectively, J·kg⁻¹·°C⁻¹.

4) Effect of temperature on the thermal conductivity of

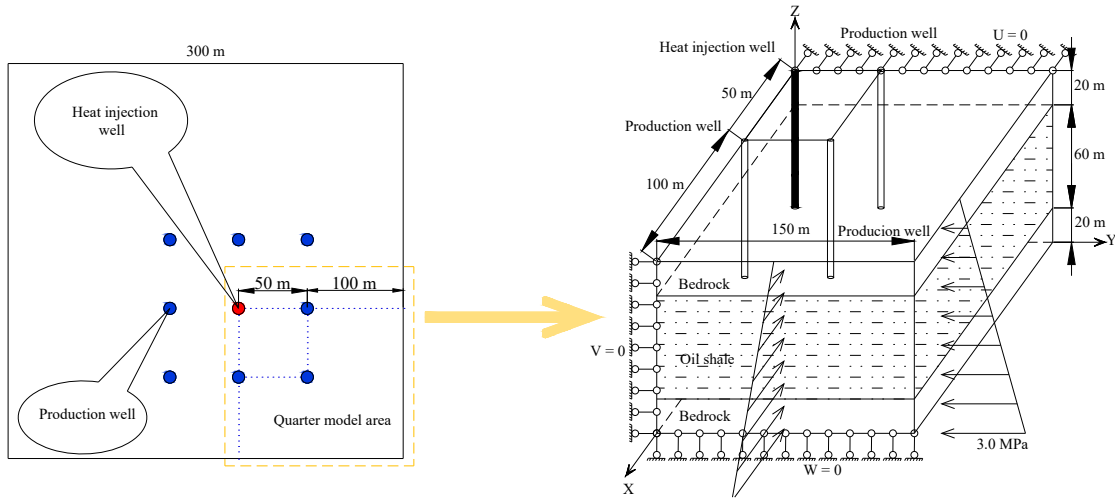


Fig. 2. Physical model of shale in situ hot exploitation process.

Table 1. Langmuir model and empirical equations for monolayer sorption.

Variable	Unit	Shale	Bedrock
Bulk density	Kg · m ⁻³	2.2 × 10 ³	3.3 × 10 ¹⁰
Elastic modulus	Pa	2.5 × 10 ¹⁰	3.3 × 10 ¹⁰
Poisson's ratio	-	0.19	0.14
Thermal conductivity	W · m ⁻¹ · C ⁻¹	2.4	1.2
Heat capacity coefficient	J · kg ⁻¹ · C ⁻¹	2.0 × 10 ³	1.2 × 10 ³
Thermal expansion coefficient	K ⁻¹	5.0 × 10 ⁻⁶	1.0 × 10 ⁻⁶
Initial permeability	m ²	2.0 × 10 ⁻¹⁷	2.2 × 10 ⁻¹⁵

water vapor and liquid water:

$$\lambda_g = 1.0 \times T^3 - 4.0 \times 10^{-6}T^2 + 0.0006T + 0.0078 \quad (28)$$

$$\lambda_w = -1.26 \times 10^{-5}T^2 + 2.56 \times 10^{-3}T + 0.5513 \quad (29)$$

where λ_g and λ_w represent the thermal conductivity of water vapor and liquid water, respectively, W · m⁻¹ · °C⁻¹.

5) Effect of temperature on shale bulk density and porosity:

$$\rho_s = 8.0 \times 10^{-9}T^3 - 9.0 \times 10^{-6}T^2 + 0.0018T + 2.0919 \quad (30)$$

$$n_s = 5.0 \times 10^{-7}T^3 + 0.0005T^2 - 0.1028T + 7.2611 \quad (31)$$

where ρ_s represents shale density, kg/m³; n_s represents shale porosity, %.

6) Effect of temperature on the thermal conductivity and specific heat of shale (Yang et al., 2020):

$$\lambda_s = \lambda_{s0} - (\lambda_{s0} - 2.01) \left[\exp\left(\frac{T - 293.15}{T + 403.15}\right) - 1 \right] \quad (32)$$

$$c_s = c_{s0}(1 + aT) \quad (33)$$

where λ_s represents the thermal conductivity of shale, W · m⁻¹ · °C⁻¹, λ_{s0} represents the thermal conductivity of shale at room temperature; c_s represents the specific heat of shale,

J · kg⁻¹ · °C⁻¹, c_{s0} represents the specific heat of shale at room temperature; a represents the temperature influence coefficient of rock specific heat, generally, $a = 3 \times 10^{-3} \text{ °C}^{-1}$.

4.2 Model construction

The simulation starts from the surface, and the study area is a 300 × 300 × 100 m cube area. Nine wells are arranged side by side on the surface, including one heat injection well and eight production wells. The spacing between all wells is 50 m, and the distance between production wells and the model boundary is 100 m, as shown in Fig. 2. According to the model's symmetry, only one-fourth of the entire region can be studied. To make the model consistent with reality, a 60-m-thick orebody in the model's middle is taken as shale and a 20-m-thick bedrock is deposited at the top and bottom. Considering significant heat loss in the bedrock, only a 60 m shale formation is selected as the heating section in the above model. Table 1 shows the basic physical parameters of shale and bedrock at room temperature.

4.3 Conditions for determining the solution of model

(1) Solid deformation conditions

The model's upper boundary is the ground surface, una-

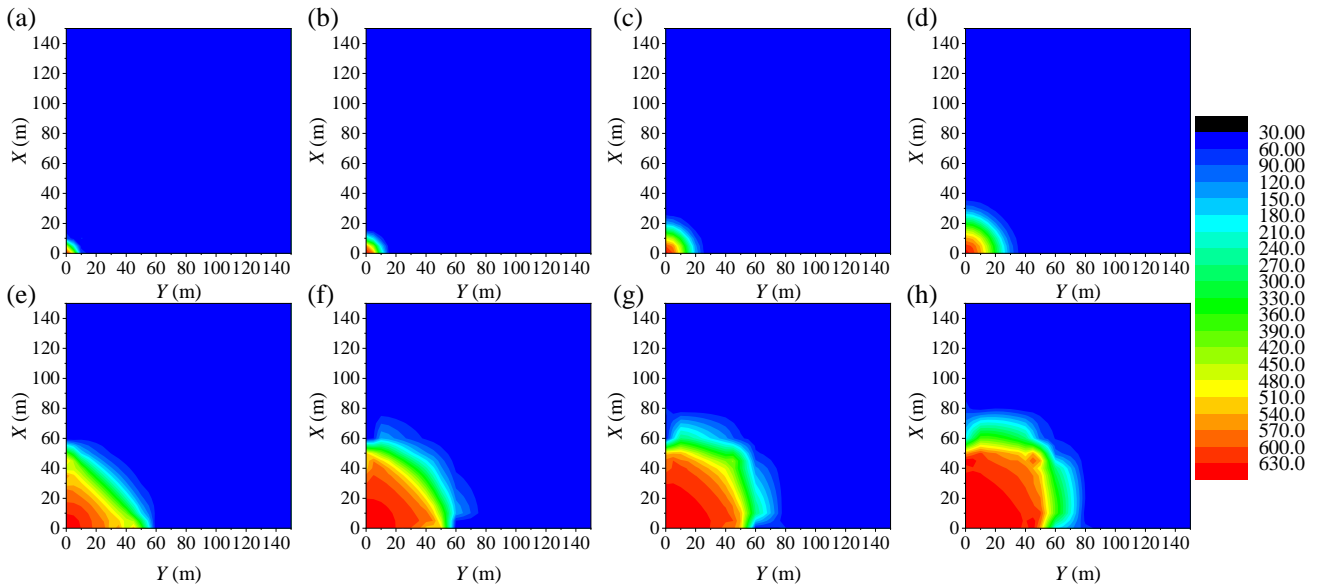


Fig. 3. Temperature distribution of section I between 0 and 2.5 years. (a) 10 days, (b) 1 month, (c) 3 months, (d) 5 months, (e) 1 year, (f) 1.5 years, (g) 2 years and (h) 2.5 years. (Unit: °C)

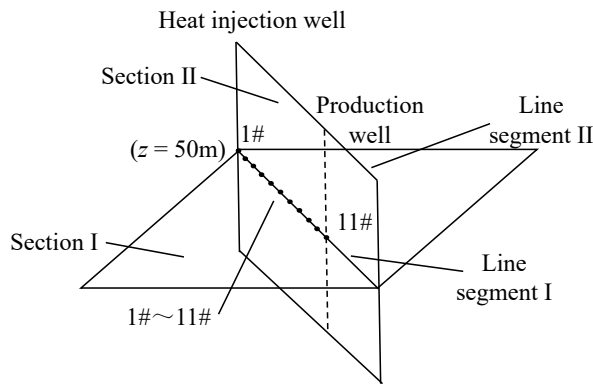


Fig. 4. Position of section, line, and point.

affected by the self-weight stress, $p_z = 0$ MPa. The surrounding rock affects the right and front model boundaries, and considering the effect of tectonic stress, reduction factors of 0.8 and 1.2 are used, $p_{x(\max)} = 2.0$ MPa, $p_{y(\max)} = 3.0$ MPa. The given boundary displacement is 0 for the other three boundaries because the boundary deformation is constrained, and the boundary conditions are simplified, as shown in Fig. 3.

(2) Boundary conditions of the seepage field

His study adopts a pressure condition, i.e., a given pressure of 3 MPa in the heat injection well, to ensure the operation of the fluid circulation system in the heat injection production. The model's upper boundary and the production well are exposed to the atmosphere, and the given pressure is 0.1 MPa. Simultaneously, the initial pore pressure in the model is 0.1 MPa. According to the model's symmetry, an impermeable boundary condition is adopted.

(3) Boundary conditions of temperature field

The initial formation temperature of the model is 30 °C, and superheated steam of 650 °C is injected into the heat

injection well. Hence, the temperature of the heat injection well is fixed at 650 °C. Because the model's upper boundary is exposed to the atmosphere, heat exchange is rapid and can be limited to 30 °C. The other boundary conditions are adiabatic.

4.4 Numerical simulation results and analysis

Here, 2 sections, 2 line segments, and 11 points are selected as the research objects to comprehensively study the distribution law of various fields of in situ shale mining. The specific spatial locations are shown in Fig. 4.

4.4.1 Dynamic change law of temperature field

Figs. 3 and 5 show the temperature distribution of sections I and II in 0-2.5 years, respectively. The closer the heat injection well, the higher the temperature in the same production time. Therefore, the closer to the heat injection well, the quicker the shale pyrolysis temperature is reached, and the pyrolysis reaction produces shale oil. After 1 year of operation, the temperature of most shale formations between thermal injection and production wells becomes < 400 °C because the main pyrolysis temperature range of shale is between 400 and 500 °C. The first year is mainly the preheating time of the formation, and the shale oil and pyrolysis gas production are less. By 2.5 years, the shale temperature in this area has reached 500 °C. The period of 1-2.5 years is a period of large shale oil and pyrolysis gas production. Most of the shale between the heat injection and production wells has been completely pyrolyzed in the 2.5 years after implementing the in situ shale mining by water vapor injection.

Fig. 6 shows an apparent preprotruding phenomenon near the three production wells, where the temperature rises rapidly. The reason is that the pressure of the fixed production well (0.1 MPa) significantly increases the pore pressure gradient near the production well. As a result, the heat transfer of fluid convection is noticeable, reflecting the coupling of the seepage

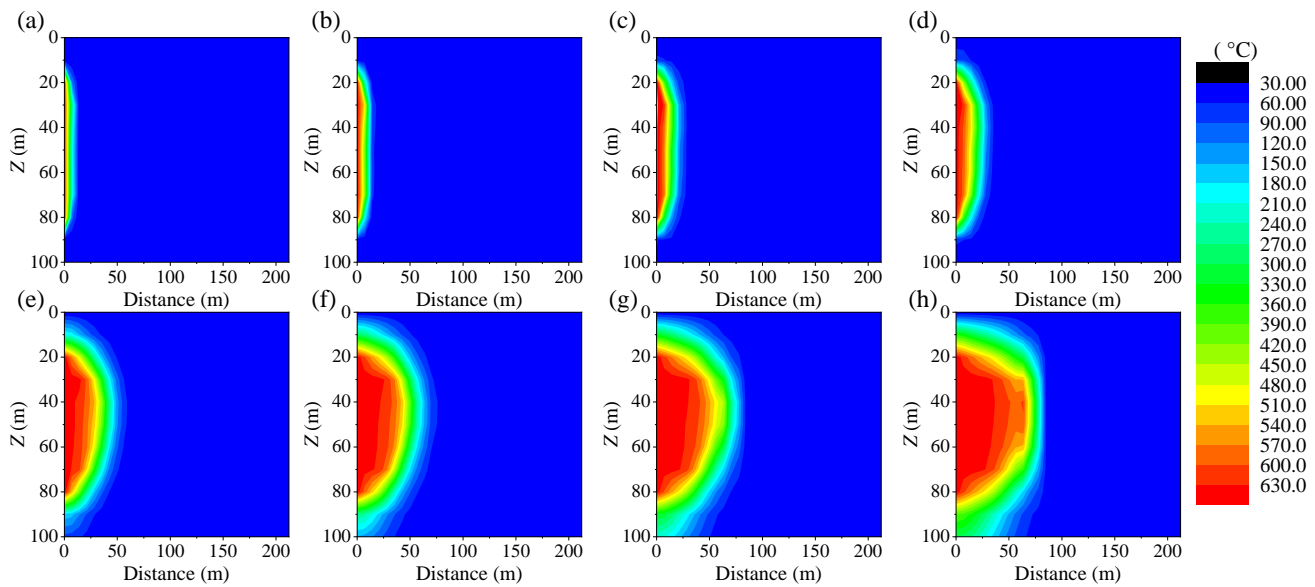


Fig. 5. Temperature distribution of section II between 0 and 2.5 years. (a) 10 days, (b) 1 month, (c) 3 months, (d) 5 months, (e) 1 year, (f) 1.5 years, (g) 2 years and (h) 2.5 years. (Unit: °C)

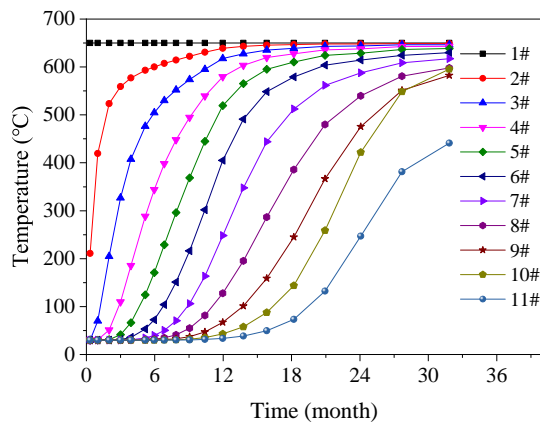


Fig. 6. Comparison between calculation solution and analytical solution.

and temperature fields. As shown in Fig. 6, the fluid convection heat transfer is significantly less than that in shale because the roof and floor rocks are far away from the heat source and their permeability coefficient is substantially lower than that of shale, resulting in considerably lower internal temperature of roof and floor rocks than that of shale. Therefore, roof and floor rock have a pronounced insulation effect and reduced heat loss. In addition, the shale temperature at 30 m from the surface rises fastest, which is related to the heat source proximity and low-permeability coefficient due to low ground stress, which is conducive to the convective heat transfer of fluid. Taking points 1#-11# in Fig. 5 as the research objects, the temperature variation curve with time is given in Fig. 6. In 2.5 years, as heat injection time increases at a constant temperature of point 1# (650 °C), the temperature of other points shows an overall upward trend. In the area near the heat injection well, the growth trend of points 2#-5# is logarithmic, which becomes flat after rapid growth. However, points 9#-11# in

the area close to the production wells increase linearly. By 2.5 years, except for the relatively low temperature at point 11#, the temperature at other points is concentrated between 550 and 650 °C.

4.4.2 Dynamic change law of seepage field

The temperature field is directly affected by the seepage field. The fluid velocity and flow in the seepage field affect the temperature field change. Therefore, it is essential to study the change law of the seepage field to operate the control system.

Figs. 7 and 8 show the pore pressure distribution of fluid in section I and section II at 0-2.5 years, respectively. Fig. 7 shows that the pore pressure takes the heat injection well as the peak value, which gradually decreases. The pressure sweep gradually expands to the area outside the production well with time. The fixed well pressure measurements show that the injection and production well pressures are 3 and 0.1 MPa, respectively. The pressure gradient is substantial, and the velocity is high in the vicinity of the two wells. However, the pressure gradient in the middle region is low, and the velocity is stable. Fig. 11 shows that the permeability of the top and bottom rocks is weaker than that of shale, and the initial pore pressure is gradually raised with a noticeable lag. With the increase in time, the rising speed of pressure in shale formation decreases. In comparison, the rising speed of pressure in the roof and floor rock increases more rapidly. By 1 year, their pressure difference is minimal and reaches a stable state.

Similarly, taking points 1#-11# in Fig. 3 as the research objects, the pressure-time curve is given, as shown in Fig. 9. During the first 10 months of heat injection, the pressure rises rapidly, reaches the maximum value at each point from 5 to 10 months, and then the curve rapidly drops. In the initial stage of heat injection, significant differences in the formation permeability are found in the seepage channel from the heat injection well to the production well. In the area near the heat

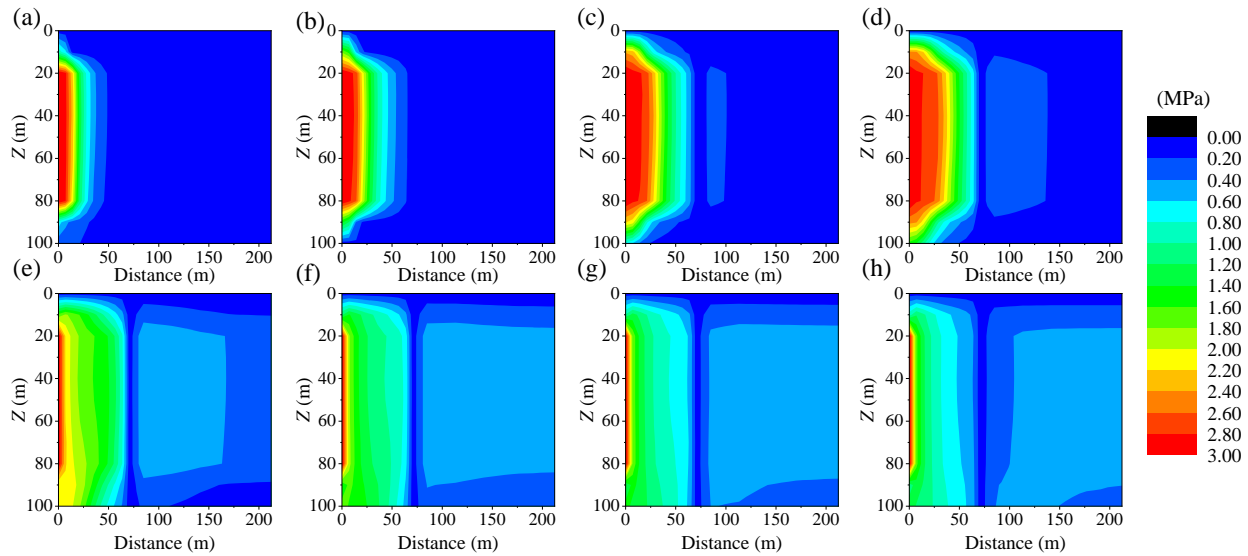


Fig. 7. Pressure distribution of section I between 0 and 2.5 years. (a) 10 days, (b) 1 month, (c) 3 months, (d) 5 months, (e) 1 year, (f) 1.5 years, (g) 2 years and (h) 2.5 years. (Unit: MPa)

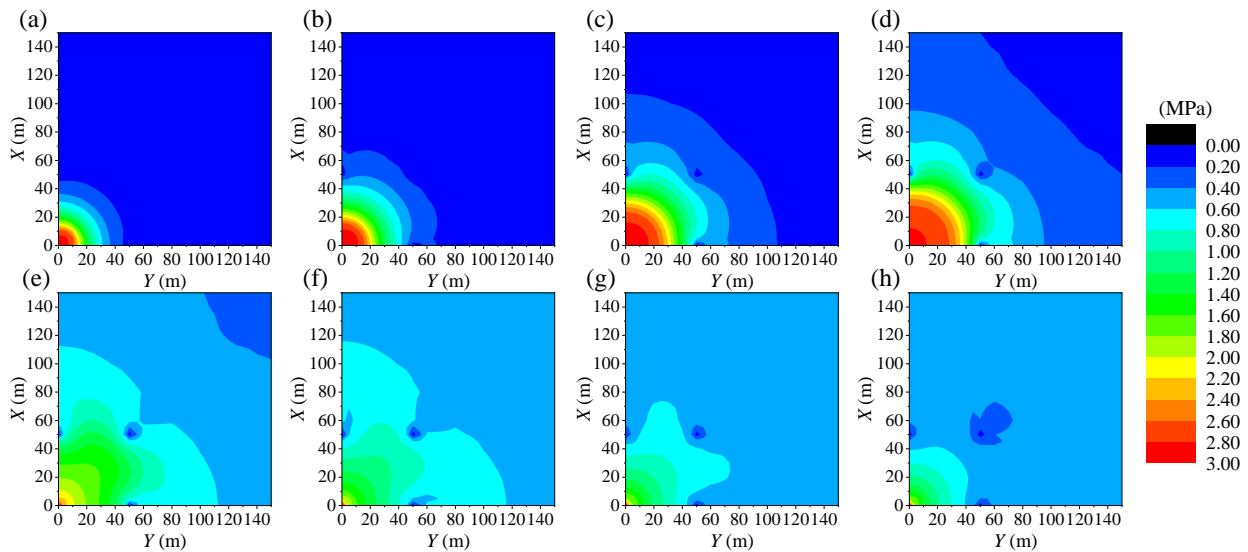


Fig. 8. Pressure distribution of section II between 0 and 2.5 years. (a) 10 days, (b) 1 month, (c) 3 months, (d) 5 months, (e) 1 year, (f) 1.5 years, (g) 2 years and (h) 2.5 years. (Unit: MPa)

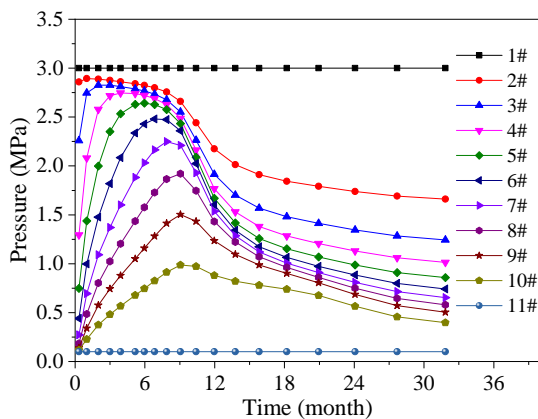


Fig. 9. $Z = 50$ m; pressure change law with time on points 1#-11#.

injection well, the shale porosity increases rapidly at high temperatures, thermal cracking is also apparent, and permeability is good. In the area near the production well, although the temperature of shale increased, its physical structure changed slightly compared with room temperature. However, the permeability is still extremely poor; therefore, the entire seepage channel is not smooth, and the fluid is easily accumulated, which is the main reason for the rapid rise of pore pressure in the initial stage of heat injection. As the formation temperature rises with time, the shale permeability near the production well is significantly improved and the entire seepage channel becomes extremely smooth after breaking through the “bottleneck.” Therefore, the accumulated pore pressure is rapidly released in a short time.

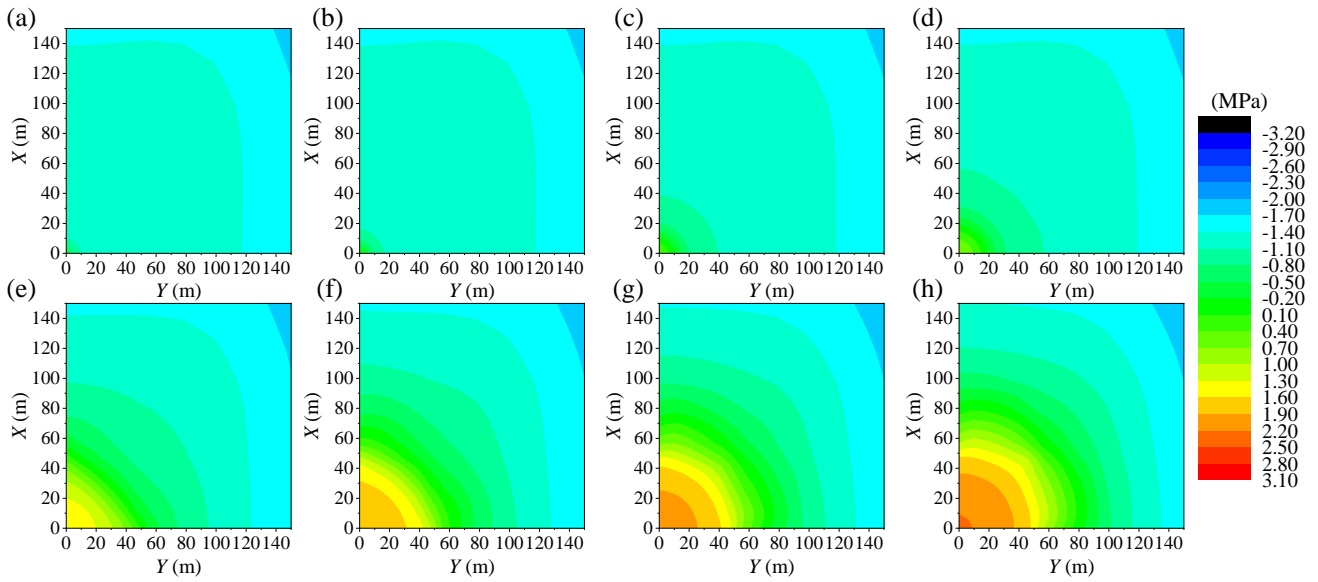


Fig. 10. σ_z distribution of section I between 0 and 2.5 years. (a) 10 days, (b) 1 month, (c) 3 months, (d) 5 months, (e) 1 year, (f) 1.5 years, (g) 2 years and (h) 2.5 years. (Unit: MPa)

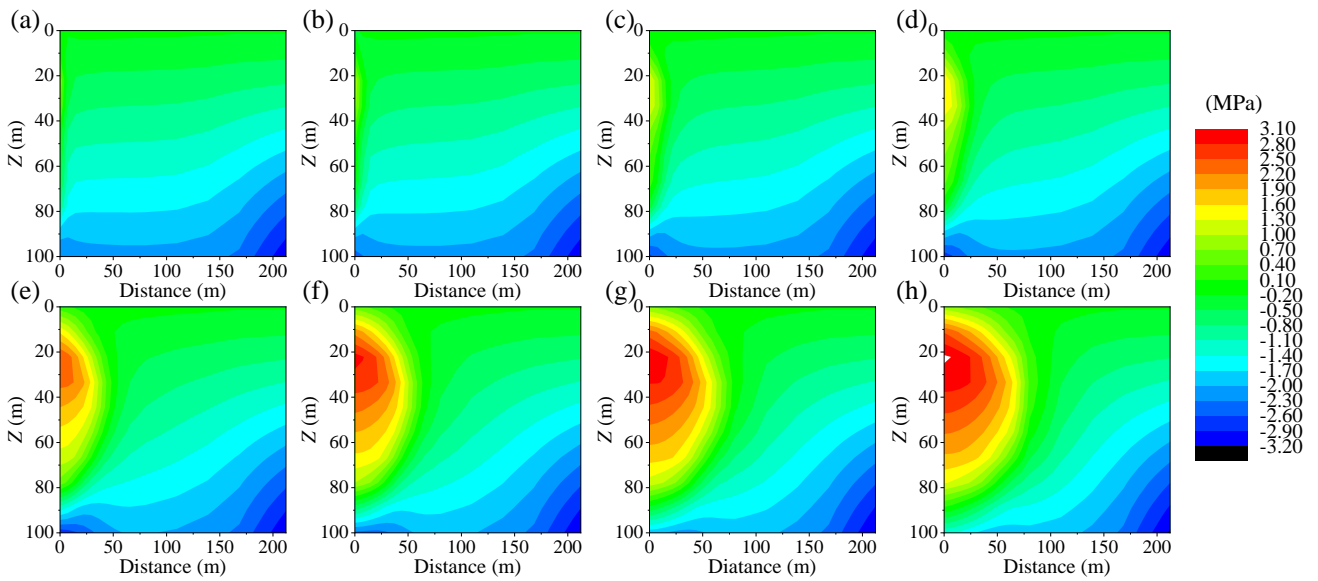


Fig. 11. σ_z distribution of section II between 0 and 2.5 years. (a) 10 days, (b) 1 month, (c) 3 months, (d) 5 months, (e) 1 year, (f) 1.5 years, (g) 2 years and (h) 2.5 years. (Unit: MPa)

4.4.3 Dynamic change law of stress field

Under the coupling effect of three fields, changing the pore pressure and temperature produces additional node load. The injected high-temperature water vapor raises the surrounding rock temperature near the heat injection well, and the surrounding rock expands and deforms, resulting in thermal stress. This behavior affects the distribution of the original stress field of rock mass and changes the opening of pores and fractures and seepage field.

Fig. 10 shows the vertical stress distribution in section I from 0 to 2.5 years. With increasing temperature, the rock mass will expand and deform, resulting in thermal stress. Moreover, the direction of thermal stress and formation gravity

stress is opposite, which counteracts each other. Hence, the vertical stress gradually evolves from compressive stress to tensile stress, and as time passes, the scope of tensile stress expands outward with the heat injection well as the center. After 5 months of operation, the vertical stress near the injection well is 0.45 MPa; by 2.5 years, there is a significant and gradual increase in vertical stress to 2.19 MPa. In the stress concentration area, one side near the heat injection well undergoes rock expansion and compression from the direction of the heat injection well. In contrast, the other side is subjected to compressive stress from the boundary. Therefore, stress concentration is inevitable in the central part.

Fig. 11 shows the vertical stress distribution in section II

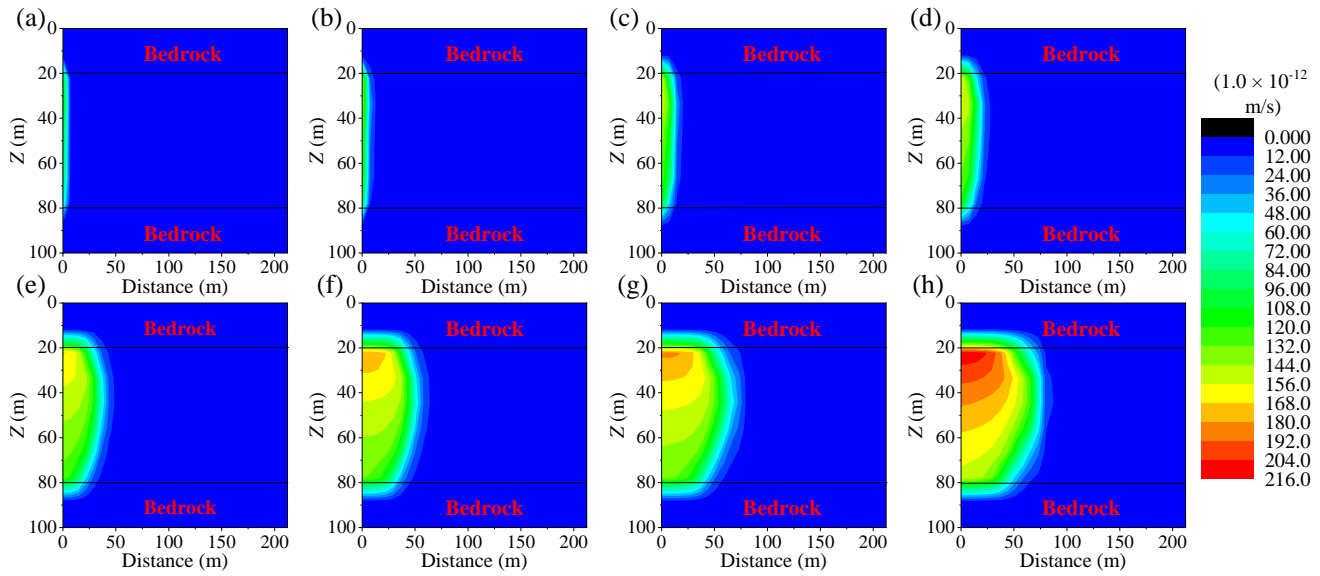


Fig. 12. Stratum permeability distribution of section II between 0 and 2.5 years. (a) 10 days, (b) 1 month, (c) 3 months, (d) 5 months, (e) 1 year, (f) 1.5 years, (g) 2 years and (h) 2.5 years. (Unit: 1.0×10^{-12} m/s)

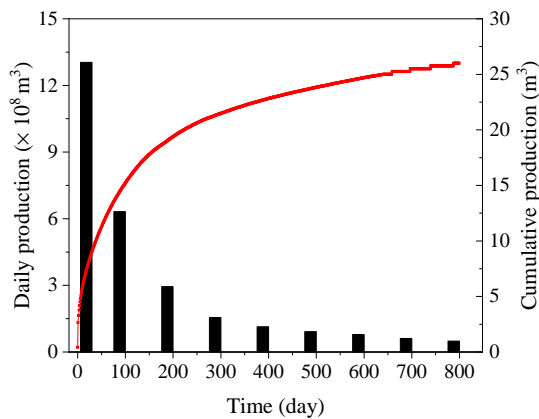


Fig. 13. Change of daily production and cumulative production over time.

from 0 to 2.5 years. The tensile stress area extends outwards with time in an approximate arc shape, with the formation being 20 m away from the surface of the heat injection well as the center. After 5 months of operation, the vertical stress at the center is 0.91 MPa, gradually increasing to 2.89 MPa in 2.5 years. With an increase in tensile stress, the pore volume increases with the fracture width, creating favorable conditions for a further injection of high-temperature water vapor.

4.4.4 Variation of formation permeability coefficient

In in situ shale mining by heat injection, the permeability coefficient is the result of multiple factors, mainly in the following three aspects: 1) The coupling effect of the stress field on the permeability coefficient is mainly reflected because the permeability coefficient is a negative exponential function of effective volume stress (the volume stress is the sum of the stresses on the rock mass in X , Y and Z directions). Therefore, it is reduced by compressive stress and increased by tensile stress. 2) The coupling effect of the temperature

field on the permeability coefficient is mainly reflected in the essential change of the shale's physical structure with an increase in temperature. An increase in porosity and thermal cracking promotes the increase in permeability coefficient. 3) The permeability coefficient is extremely sensitive to the change in fluid viscosity. In general, liquid water viscosity is thousands of times that of water vapor. Therefore, with the continuous injection of water vapor, the viscosity of fluid decreases and the permeability coefficient of formation is significantly improved.

Fig. 12 shows the distribution of the formation permeability coefficient in section II from 0 to 2.5 years. In the initial stage of heat injection under the control of in situ stress, the permeability coefficient shows pronounced stratification, except for local fluctuation, which decreases with increasing formation depth. The variation range of the permeability coefficient of the roof and floor rock is from 0.01×10^{-12} to 0.1×10^{-12} m/s and that of shale formation is from 1.0×10^{-12} to 3.0×10^{-12} m/s. With the continuous injection of heat under the above three factors, the permeability coefficient of the formation made a qualitative leap and the original layered distribution law was disturbed. The permeability coefficient shows an approximately circular shape extending from the heat injection well to its surroundings. By 2.5 years, the variation range of the permeability coefficient is from 30×10^{-12} to 212×10^{-12} m/s, nearly 100 times more than the original state.

5. Yield analysis

Fig. 13 shows the daily and cumulative production of orebody products. Shale oil and gas production can be divided into two stages. The first stage (0-200 d) is the main stage of shale oil and gas production. High-temperature steam can heat the reservoir at a higher rate to complete the pyrolysis of the reservoir. In the second stage (200-800 d), the daily output of shale oil and gas remains at a low level.

6. Conclusion

Based on a theoretical analysis, a thermohydronechanical coupling mathematical model for in situ exploitation of shale is developed. Its numerical solution is obtained, providing a theoretical basis for analyzing and solving the complex physical and chemical processes of in situ shale mining by heat injection. From the mathematical model compiled in FORTRAN programming language, the numerical simulation of a well group with a “nine-point method” well layout under in situ shale mining by water vapor injection is performed.

- 1) When the system's operation time increases from 1 to 2.5 years, the temperature of most shale formations between heat injection and production wells increases from 400 to 500 °C. Therefore, the period of 1-2.5 years produces considerable amounts of shale oil and pyrolysis gas.
- 2) The pore pressure takes the heat injection well as the peak value and gradually decreases. The scope of the pressure sweep gradually expands with time to the area outside the production well.
- 3) Vertical stress gradually evolves from compressive to tensile stress with increasing temperature. The scope of tensile stress expands outwards with time with the center of the heat injection well. With increasing tensile stress, the pore volume and fracture width increase, creating favorable conditions for the further injection of high-temperature water vapor.
- 4) At the initial stage of heat injection, the permeability coefficient shows pronounced stratification, which decreases with increasing formation depth. As a result, the permeability coefficient of shale formation varies from 1.0×10^{-12} to 3.0×10^{-12} m/s. The permeability coefficient shows an approximately circular shape with time, extending from the heat injection well to its surroundings. By 2.5 years, the permeability coefficient of shale formation in the area between the heat injection and production wells increases nearly 100 times.

Acknowledgements

This work was funded by National Natural Science Foundation of China (Nos. 52104144, 11772213) and National Key R&D Program of China (Nos. 2019YFA0705501, 2019YFA0705502). We thank Shiyanjia Lab (www.shiyanjia.com) for its linguistic assistance during the preparation of this manuscript.

Conflict of interest

The authors declare no competing interest.

Open Access This article is distributed under the terms and conditions of the Creative Commons Attribution (CC BY-NC-ND) license, which permits unrestricted use, distribution, and reproduction in any medium, provided the original work is properly cited.

References

- Akinlua, A., Smith, R. M. High temperature steam extraction for the determination of aliphatic hydrocarbons in petroleum source rock. *Chromatographia*, 2009, 69(11): 1333-1339.
- Avraam, D. G., Payatakes, A. C. Flow regimes and relative permeabilities during steady-state two-phase flow in porous media. *Journal of Fluid Mechanics*, 1995, 293: 207-236.
- Bansal, V. R., Kumar, R., Sastry, M. I. S., et al. Direct estimation of shale oil potential by the structural insight of Indian origin kerogen. *Fuel*, 2019, 241: 410-416.
- Biot, M. A. General theory of three-dimensional consolidation. *Journal of Applied Physics*, 1941, 12: 144-164.
- Gelet, R., Loret, B., Khalili, N. Borehole stability analysis in a thermoporoelastic dual-porosity medium. *International Journal of Rock Mechanics and Mining Sciences*, 2012, 50: 65-76.
- Kang, Z., Zhao, Y., Yang, D. Review of oil shale in-situ conversion technology. *Applied Energy*, 2020, 269: 115121.
- Kelkar, S., Lewis, K., Karra, S., et al. A simulator for modeling coupled thermo-hydro-mechanical processes in subsurface geological media. *International Journal of Rock Mechanics and Mining Sciences*, 2014, 70: 569-580.
- Li, H., Pan, C., Miller, C. T. Pore-scale investigation of viscous coupling effects for two-phase flow in porous media. *Physical Review E*, 2005, 72(2): 026705.
- Liang, W., Zhao, Y., Liu, J., et al. Advances in in-situ modified mining by fluidization and in unconventional geomechanics. *Advances in Geo-Energy Research*, 2021, 5(1): 1-4.
- Lin, L., Lai, D., Guo, E., et al. Oil shale pyrolysis in indirectly heated fixed bed with metallic plates of heating enhancement. *Fuel*, 2016, 163: 48-55.
- Montgomery, W., Court, R. W., Rees, A. C., et al. High temperature reactions of water with heavy oil and bitumen: Insights into aquathermolysis chemistry during steam-assisted recovery. *Fuel*, 2013, 113: 426-434.
- Nur, A., Byerlee, J. D. An exact effective stress law for elastic deformation of rock with fluids. *Journal of Geophysical Research*, 1971, 76(26): 6414-6419.
- Pei, S., Wang, Y., Zhang, L., et al. An innovative nitrogen injection assisted in-situ conversion process for oil shale recovery: Mechanism and reservoir simulation study. *Journal of Petroleum Science and Engineering*, 2018, 171: 507-515.
- Raeini, A. Q., Blunt, M. J., Bijeljic, B. Modelling two-phase flow in porous media at the pore scale using the volume-of-fluid method. *Journal of Computational Physics*, 2012, 231(17): 5653-5668.
- Rao, X., Xu, Y., Liu, D., et al. A general physics-based data-driven framework for numerical simulation and history matching of reservoirs. *Advances in Geo-Energy Research*, 2021, 5(4): 422-436.
- Saif, T., Lin, Q., Gao, Y., et al. 4D in situ synchrotron X-ray tomographic microscopy and laser-based heating study of oil shale pyrolysis. *Applied Energy*, 2019, 235: 1468-1475.
- Salimzadeh, S., Paluszny, A., Nick, H. M., et al. A three-dimensional coupled thermo-hydro-mechanical model for deformable fractured geothermal systems. *Geothermics*,

- 2018, 71: 212-224.
- Saurel, R., Abgrall, R. A multiphase Godunov method for compressible multifluid and multiphase flows. *Journal of Computational Physics*, 1999, 150(2): 425-467.
- Shabdirova, A., Minh, N. H., Zhao, Y. A sand production prediction model for weak sandstone reservoir in Kazakhstan. *Journal of Rock Mechanics and Geotechnical Engineering*, 2019, 11(4): 760-769.
- Suganuma, S., Katada, N. Innovation of catalytic technology for upgrading of crude oil in petroleum refinery. *Fuel Processing Technology*, 2020, 208: 106518.
- Sultana, K., Rahman, M. T., Habib, K., et al. Recent advances in deep eutectic solvents as shale swelling inhibitors: A comprehensive review. *ACS Omega*, 2022, 7(33): 28723-28755.
- Sun, Y., Kang, S., Wang, S., et al. Subcritical water extraction of Huadian oil shale at 300 °C. *Energy & Fuels*, 2019, 33(3): 2106-2114.
- Sun, X., Xu, B., Qian, G., et al. The application of geomechanical SAGD dilation startup in a Xinjiang oil field heavy-oil reservoir. *Journal of Petroleum Science and Engineering*, 2021, 196: 107670.
- Tong, F., Jing, L., Zimmerman, R. W. A fully coupled thermo-hydro-mechanical model for simulating multiphase flow, deformation and heat transfer in buffer material and rock masses. *International Journal of Rock Mechanics and Mining Sciences*, 2010, 47(2): 205-217.
- Wang, G., Liu, S., Yang, D., et al. Numerical study on the in-situ pyrolysis process of steeply dipping oil shale deposits by injecting superheated water steam: A case study on Jimsar oil shale in Xinjiang, China. *Energy*, 2022, 239: 122182.
- Wang, G., Yang, D., Kang, Z., et al. Numerical investigation of the in situ oil shale pyrolysis process by superheated steam considering the anisotropy of the thermal, hydraulic, and mechanical characteristics of oil shale. *Energy & Fuels*, 2019, 33(12): 12236-12250.
- Wang, L., Yang, D., Kang, Z. Evolution of permeability and mesostructure of oil shale exposed to high-temperature water vapor. *Fuel*, 2021, 290: 119786.
- Wang, L., Zhao, Y. S., Yang, D. Investigation on meso-characteristics of in-situ pyrolysis of oil shale by injecting steam. *Chinese Journal of Rock Mechanics and Engineering*, 2020, 39(8): 1634-1647. (in Chinese)
- War, K., Arneppalli, D. N. A review on coupled phenomena in aquifers from the perspective of geological storage of carbon dioxide with ecological significance. *Building Materials for Sustainable and Ecological Environment*, 2021: 135-149.
- Wei, X., Feng, Z., Zhao, Y. Numerical simulation of thermo-hydro-mechanical coupling effect in mining fault-mode hot dry rock geothermal energy. *Renewable Energy*, 2019, 139: 120-135.
- Wilkins, A., Green, C. P., Ennis-King, J. An open-source multiphysics simulation code for coupled problems in porous media. *Computers & Geosciences*, 2021, 154: 104820.
- Wopara, O. F. Geochemical properties of shale gas reservoirs and their impacts on gas development: A review. *International Journal of Multidisciplinary and Current Educational Research (IJM CER)*, 2021, 3(2): 154-165.
- Yang, D., Wang, G., Kang, Z., et al. Experimental investigation of anisotropic thermal deformation of oil shale under high temperature and triaxial stress based on mineral and micro-fracture characteristics. *Natural Resources Research*, 2020, 29(6): 3987-4002.
- Yang, D., Wang, L., Zhao, Y., et al. Investigating pilot test of oil shale pyrolysis and oil and gas upgrading by water vapor injection. *Journal of Petroleum Science and Engineering*, 2021, 196: 108101.
- Yang, D., Zhao, Y., Kang, Z. Numerical simulation of in situ exploitation of oil shale by injecting high-temperature steam. *Oil Shale*, 2019, 36(4): 483-500.
- Zhao, Y. S., Feng, Z. C., Yang, D., et al. The method for mining oil & gas from oil shale by Convection heating. *CN200510012473*, 2005.